DEVELOPMENT AND VALIDATION OF A SAFETY ARCHITECTURE OF A WHEELED MOBILE DRIVING SIMULATOR

Alexander Betz[1], Paul Wagner[1], Torben Albrecht[1] , Hermann Winner[1]

(1) : Institute of Automotive Engineering, Technische Universität Darmstadt,
Otto-Berndt-Str. 2, 64287 Darmstadt, Germany
Phone: +49 (0) 6151-16-3796
Fax: +49 (0) 6151-16-5192
betz@fzd.tu-darmstadt.de, wagner@fzd.tu-darmstadt.de, torben.albrecht@stud.tu-darmstadt.de, winner@fzd.tu-darmstadt.de

Abstract – The safety architecture of the Wheeled Mobile Driving Simulator (WMDS) is not yet known. It has to cope with carrying subjects on an unbound motion base while providing safety for the users, the system, and the surroundings. The complexity of the safety architecture increases when compared to rail guided Driving Simulators (DS) since stop dampers cannot be provided for all possible impact angles and positions. A representative solution is developed and validated. The validity of the safety architecture is analyzed by hardware testing. A representative WMDS is developed for this purpose. The introduced safety architecture is derived from a Failure Mode and Effects Analysis (FMEA) and a Fault Tree Analysis (FTA). The conducted tests validate the safety architecture with respect to the discharge process and the achieved mean deceleration during the emergency stop.

Key words: Wheeled Mobile Driving Simulator, Safety System, Hardware Testing, Conception and Design, Validation.

1. Introduction

1.1. Motivation for Wheeled Mobile Driving Simulators (WMDS)

DS are an indispensable developmental tool in the automotive industry due to their high degree of reproducibility and safety. In order to fulfill the increased requirements of modern-day DS [Bet12a], a state-of-the-art DS must provide up to 12 degrees of freedom (DOF) whilst comprising of multiple drive mechanisms. These improvements come with the disadvantage of creating a complex system with an increased moving mass of about 80 t [Cla01]. Thus, a link between moving mass and motion envelope is created, limiting either motion envelope or system dynamics.

This dilemma has been recognized by the automotive industry, as attested by Zeeb in 2010, former head of Driving Simulators at Daimler: "*To induce a much better longitudinal motion sensation with a scaling factor close to 1:1 for all possible acceleration and deceleration scenarios even a several ten meter long sledge would not be sufficient, but would increase the technical and financial effort tremendously, especially when the […] mandatory requirements for drive dynamic experiments have to be fulfilled.*" [Zee10].

Another aspect is the limited yaw angle in advanced dynamic DS. Urban traffic maneuvers like parking, turning, or reversing require great yaw that cannot be provided adequately by state of the art advanced dynamic DS.

Mobile dynamic DS, like the WMDS, solve the core problem of the increased moving mass and provide unlimited yaw motion.

1.2. Presentation of the WMDS Concept

The proposed design of a WMDS shows three self-propelled and active steerable wheels that allow horizontal motion and yaw [Bet10, Bet14]. The main idea is based on the assumption that a wheeled system, whose propulsion is limited by friction forces, is suitable to simulate the horizontal dynamics of vehicles that are also limited by tire friction forces.

An additional system provides at minimum cabin tilt and heave. Avoiding the conventional rail systems, which mainly cause the moving mass to increase, results in a light weight concept [Bet12a, Bet12b]. The design and con-

struction of the WMDS are carried out at the Institute of Automotive Engineering (Fahrzeugtechnik Darmstadt: FZD), Technische Universität Darmstadt, Germany since 2010.

A multi-body simulation [Bet13] as well as a scaled hardware prototype of the WMDS was built in 2013 [Wag13, Wag14, Bet14]. The hardware prototype is currently in operation at FZD. A photograph of the prototype can be seen in Fig. 1, where the hexapod is situated in the middle of the omnidirectional platform. The illustrated user-machine-interface is not intended to be applied for DS studies but presents the final position of the DS cabin. Furthermore the drive units with its steering and traction motors are visible. The system does not contain friction brakes and uses only the electric motors as service brakes.

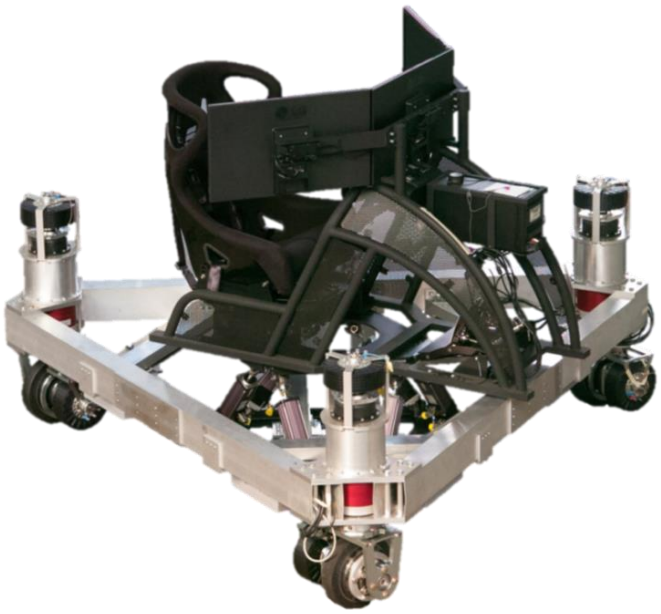

Fig. 1: Assembled scaled WMDS prototype

1.3. Motivation for a WMDS Safety System

The safety architecture is a vital element of a DS since the simulator must cope with carrying subjects on a motion base while providing safety for the users, the system, and the surroundings. The unbound characteristic of the WMDS increases the complexity of the safety architecture compared to rail guided DS. This increase is because conventional stop dampers cannot be provided for all possible impact angles and positions of the unbound system.

Most of the components used for the prototype are prototypical themselves, barely researched, or custom-made items. Hence, most components are not released for safety critical applications. Even the chosen tires are barely researched although they are derived from volume production in the forklift truck industry.

1.4. Methodology

The requirements of the safety architecture are derived by a FMEA and the FTA. The FTA is based on a critical top event for a countermeasure found by the FMEA. [Bet14]

A representative solution for the safety architecture of the WMDS is developed and a physical reference system is build up. Hardware tests analyze the performance of the representative solution and thereby validate the chosen architecture.

This safety architecture countermeasures the amount of considered failures and paves the way for the first test drives with the worldwide unprecedented WMDS prototype.

2. Concept Idea

The results of the FMEA lead to the conclusion that an additional system is required to avoid the potential failure modes of the overall WMDS prototype. The idea is to lift the system off the ground and thereby decoupling the drive units from the ground. Thus, the drive train of the WMDS is cut. This helps to prevent consequences from corrupt or incorrect motor actions independent from the manifold error sources (software, data transfer, energy supply, hardware, etc.).

Still there is potential hazard from the kinetic energy of the WMDS as long as the system is in motion. The safety architecture relocates the contact forces from the wheels to new elements of the lifting system. In order to provide deceleration those elements have to generate horizontal force in opposite direction to the velocity vector of the contact point.

Several technical solutions are available for creating this decelerating force. Nevertheless, friction based force transmission is highly appropriate in terms of low complexity, low mass and low cost. The wear of the friction elements is expected to be tolerable because the system represents an emergency stop system and not a service brake.

It must be considered that the new contact patches, where the deceleration force is generated, take over the responsibility for rollover safety. Hence, the number (at least three) and position of the new contact patches underlie similar constraints like the positioning of the drive units [Wag14]. The question arises how the system lift and the decelerating force is generated. It must be stressed that no existing example of the presented safety architecture is known. Thus, the physical reference system is expected to serve as a research prototype that

accelerates the gain of system understanding by hardware testing. The representative solution is introduced hereafter.

3. FTA of Safety Architecture

In the safety architecture, the friction force created as well as the support force of the mountings are subject to the friction coefficient, contact force, and force transmission. Therefore, the top event of the FTA must treat the event chain of those forces. The result of the FTA is presented in Fig. 2.

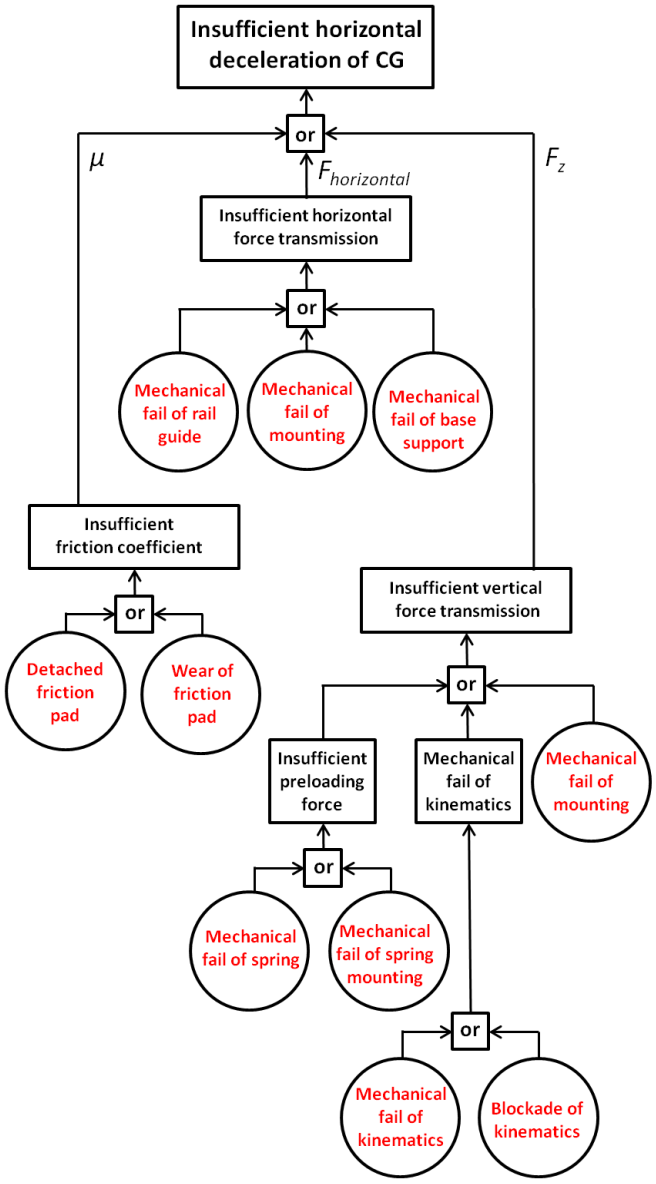

Fig. 2: FTA of critical top event [Bet14]

The controllability of the critical failures that cause the top event is realized by safety factors in the dimensioning process and a redundancy of the utilized number of lifting systems. Hence, six lifting systems are applied (see Fig. 3, two at each edge of the triangle) instead of the minimum required number of three systems.

4. Representative Solution

4.1. Concept

The representative solution utilizes friction forces of the new contact patches. Therefore, friction pads are used. Those forces result from contact forces and sliding friction created by a relative velocity of the new contact patches with respect to the ground. According to Fig. 3, the contact force is created by a knee lever that is actuated by a spring. The spring provides the needed energy for lifting the WMDS prototype off the ground. In order to ensure the lifting even in case of an electrical outage, the spring is preloaded before the start of operation and is hold actively by electromagnetic clamps. If any internal functional error (software or electrical) or fault is detected, the tolerated workspace is left, or any of the emergency stops is activated, the electrical circuit of the magnets is cut and the passive lifting task is initiated. Fig. 3 illustrates the hold (left) and emergency position (right) of the lifting system.

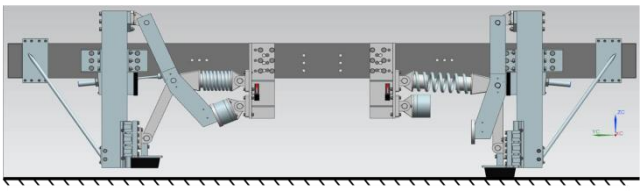

Fig. 3: CAD model of the lifting system (left: actively held; right: discharged)

4.2. Analysis of Lifting Stroke and Lifting Force Demand

The inverting of the activation logic increases the reliability of the safety architecture but causes continuous power demand for holding the preloaded spring. The force demand for lifting the WMDS is not linear with respect to vertical displacement, thus, a conventional spring with its linear characteristics is not the most suitable component, as shown in Fig. 4 by an exemplarily chosen spring characteristic providing the demanded force at maximum lifting stroke (dotted graph). In the actively held position, the lifting system has a desired initial lifting force of zero since no contact force at the friction element exists. This relation is valid for about 10 mm because this is the space required as ground clearance during operation (see left side of Fig. 3). After the gap has been closed by the safety system, the friction pad touches the ground and lifting force is thereby generated. After the gap has been closed, the created lifting force of the friction elements reduces the wheel loads. This phase of the lifting procedure is approximated by a

linear characteristic[1]. The maximum desired lifting force is derived by a worst-case assumption concerning maximum wheel load (8688 N) due to assumed peak tire friction (μ_{max} = 1.45). As soon as all wheels have lost their ground contact no further increase of lifting force is necessary. However, further lift is desired to cause a defined tire-ground clearance for the emergency brake phase. As mentioned before and confirmed by the solid graph of Fig. 4, the discussed force demand does not meet conventional spring characteristics. The overall stroke of the lifting system is about 40 mm.

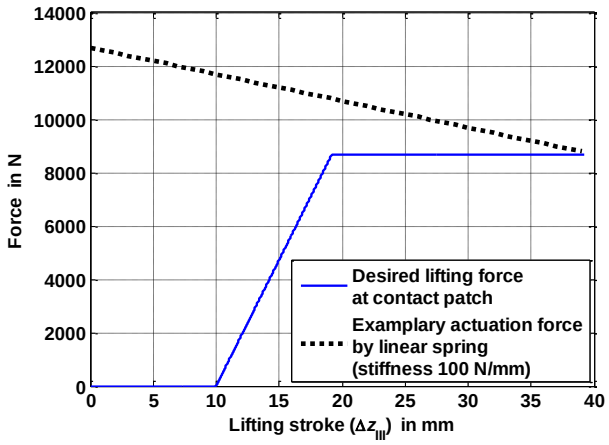

Fig. 4: Desired lifting force at contact patch and actuation force

4.3. Application of a Knee Lever

The desired force characteristic is realized by a conventional spring that acts on a knee lever. The non-linear transmission ratio of the knee lever in combination with a linear spring results in a non-linear force characteristic with respect to the lifting stroke. According to Fig. 5, the corresponding equations (1) to (24) apply.

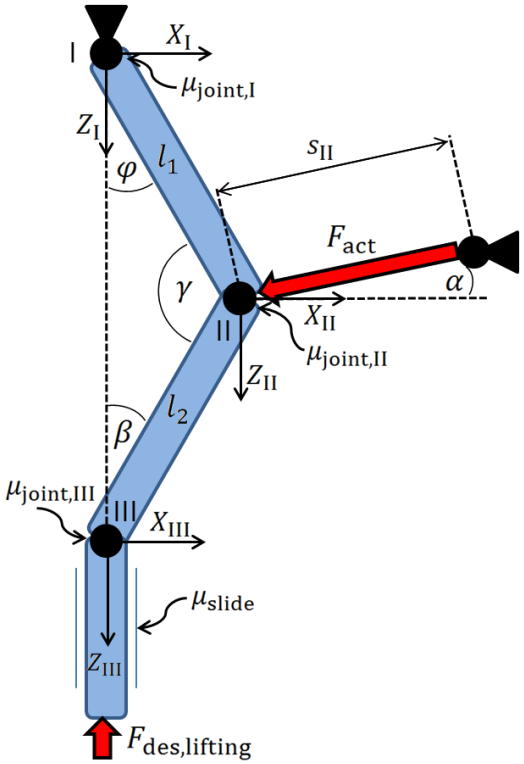

Fig. 5: Knee lever setup with lifting force and actuation force

The following relationship is derived using the law of energy conservation and accounts only for the discharge motion of the safety architecture:

$$\mathrm{d}z_{\mathrm{III}} F_{\mathrm{des}} = F_{\mathrm{act}} \mathrm{d}s_{\mathrm{II}} \tag{1}$$

Considering friction and the angle of the actuation force, equation (1) yields equations (2) to (6).

$$F_{\mathrm{des}}\mathrm{d}z_{\mathrm{III}} + F_{\mathrm{frict,slide}}\mathrm{d}z_{\mathrm{III}} + M_{\mathrm{fric,joint,I}}\mathrm{d}\varphi + M_{\mathrm{fric,joint,III}}\mathrm{d}\beta + M_{\mathrm{fric,joint,II}}\mathrm{d}\gamma = F_{\mathrm{act}}\left[\cos(\alpha)\mathrm{d}x_{\mathrm{II}} + \sin(\alpha)\mathrm{d}z_{\mathrm{II}}\right] \tag{2}$$

$$F_{\mathrm{frict,slide}} = \mu_{\mathrm{slide}} F_{x,\mathrm{III}} \tag{3}$$

$$M_{\mathrm{fric,joint,I}} = \mu_{\mathrm{joint}} \frac{d}{2} F_{l1} \tag{4}$$[2]

$$M_{\mathrm{fric,joint,II}} = \mu_{\mathrm{joint}} \frac{d}{2} F_{\mathrm{act}} \tag{5}$$[2]

$$M_{\mathrm{fric,joint,III}} = \mu_{\mathrm{joint}} \frac{d}{2} F_{l2} \tag{6}$$[2]

The unknown forces of equation (7), (8) and (9) are derived from a free-body diagram, Fig. 6. For the sake of readability u_1, u_2 and u_3 are introduced.

$$F_{x,\mathrm{III}} = F_{\mathrm{act}}(\cos(\alpha) - u_1) \tag{7}$$

[1] Vertical tire stiffness according to experimental test on the GUMASOL test facility (28.06.2013): 1036 N/mm (linearized spring rate)

[2] [Ker12]

$$F_{l1} = F_{\text{act}} u_2 + F_{\text{des}} \cos(\varphi) \quad (8)$$

$$F_{l2} = F_{\text{act}} u_3 + F_{\text{des}} \cos(\beta) \quad (9)$$

$$u_1 = \frac{\cos(\alpha+\beta)}{\cos(\varphi) l_1 + \cos(\beta) l_2} l_2 \quad (10)$$

$$u_2 = \sin(\varphi) u_1 + \cos(\varphi)\,(\mu_{\text{slide}}(\cos(\alpha) - u_1) - \sin(\alpha)) \quad (11)$$

$$u_3 = (\cos(\alpha) - u_1)(\sin(\beta) + \mu_{\text{slide}} \cos(\beta)) \quad (12)$$

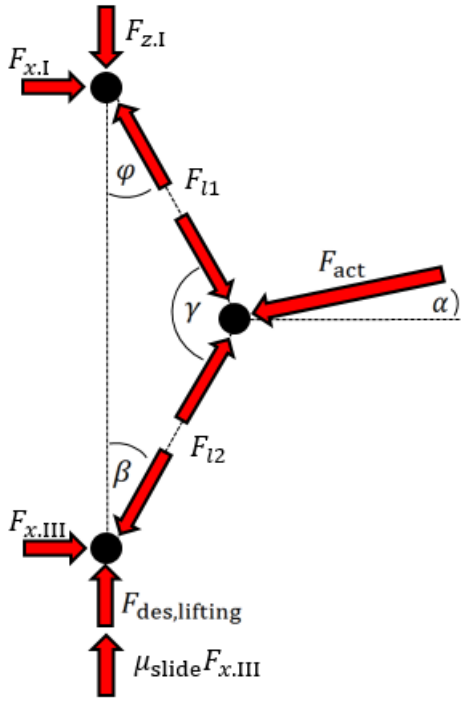

Fig. 6: Free body diagram of knee lever

The normal force $F_{x,\text{III}}$ (7), needed to calculate the frictional forces in the sliding joint (3), is derived by the sum of forces in x-directions (14), the reaction force $F_{x,\text{I}}$ (24) by the sum of moments about joint III (13). The rod forces F_{l1} (9) and F_{l2} (8), used to determine the frictional moments (4) and (6) in the joints, are derived by the sum of forces at joint I (17) and III (18) in direction of l_1 and l_2.

The sum of moments about joint III yields:

$$F_{x.\text{I}}(\cos(\varphi)\, l_1 + \cos(\beta)\, l_2) = F_{\text{act}} \cos(\alpha) \cos(\beta)\, l_2 - F_{\text{act}} \sin(\alpha) \sin(\beta)\, l_2$$

$$\rightarrow F_{x.\text{I}} = F_{\text{act}} \frac{\cos(\text{á}) \cos(\beta) - \sin(\alpha)\sin(\beta)}{\cos(\varphi) \cdot l_1 + \cos(\beta) \cdot l_2} l_2 = F_{act} \cdot u_1 \quad (13)$$

The sum of forces in x-direction yields:

$$F_{x.\text{I}} + F_{x.\text{III}} = F_{\text{act}} \cdot \cos(\alpha)$$

$$F_{x.\text{III}} = F_{\text{act}} \left(\cos(\alpha) - \frac{\cos(\alpha)\cos(\beta) - \sin(\alpha)\sin(\beta)}{\cos(\varphi) \cdot l_1 + \cos(\beta) \cdot l_2} l_2 \right)$$

$$\rightarrow F_{x.\text{III}} = F_{\text{act}}(\cos(\alpha) - u_1) \quad (14)$$

The sum of forces in z-direction yields:

$$F_{z.\text{I}} + \sin(\alpha) F_{\text{act}} = F_{\text{des}} + \mu_{\text{slide}} F_{x.\text{III}} \quad (15)$$

$$\rightarrow F_{z.\text{I}} = F_{\text{des}} + F_{\text{act}}(\mu_{\text{slide}}(\cos(\alpha) - u_1) - \sin(\alpha)) \quad (16)$$

The sum of forces at joint I in F_{l1}-direction yields:

$$F_{l1} = \sin(\varphi)\, F_{x.\text{I}} + \cos(\varphi)\, F_{z.\text{I}}$$

$$= F_{\text{act}}\big(\sin(\text{ö}) u_1 + \cos(\varphi)\,(\mu_{\text{slide}}(\cos(\alpha) - u_1) - \sin(\alpha))\big) + \cos(\varphi)\, F_{\text{des}}$$

$$\rightarrow F_{l1} = F_{\text{act}} u_2 + F_{\text{des}} \cos(\varphi) \quad (17)$$

The sum of forces at joint III in F_{l2}-direction yields:

$$F_{l2} = \sin(\beta)\, F_{x.\text{III}} + \cos(\beta)\, F_{\text{des}} + \cos(\beta)\, \mu_{\text{slide}} F_{x.\text{III}}$$

$$= F_{\text{act}}(\cos(\alpha) - u_1)(\sin(\beta) + \cos(\beta)\, \mu_{\text{slide}}) + \cos(\beta)\, F_{\text{des}}$$

$$\rightarrow F_{l2} = F_{\text{act}} u_3 + F_{\text{des}} \cos(\beta) \quad (18)$$

Considering equations (2) to (12) leads to the final relation of the actuation force (19). The differential displacements are unambiguously related by geometrical constraints of the knee lever and result in variable transmission with respect to the knee levers state – φ (equations (20) to (24)).

$$F_{\text{act}} = \frac{F_{\text{des}} \left[\text{d}z_{\text{III}} + \mu_G \frac{d}{2} (\cos(\beta)\, \text{d}\beta + \text{d}\varphi) \right]}{\cos(\alpha) \text{d}x_{\text{II}} + \sin(\alpha) \text{d}z_{\text{II}} - \mu_{\text{slide}}(\cos(\alpha) - u_1) \text{d}z_{\text{III}} - \mu_{\text{joint}} \frac{d}{2} [u_2 \text{d}\varphi + u_3 \text{d}\beta + d\gamma]} \quad (19)$$

$$x_{\text{II}} = \sin(\varphi)\, l_1 \quad (20)$$

$$z_{\text{II}} = \cos(\varphi) l_1 \quad (21)$$

$$z_{\text{III}} = \cos(\varphi) l_1 + \sqrt{l_2^2 - (\sin(\varphi)\, l_1)^2} \quad (22)$$

$$\sin(\beta) = \sin(\varphi) \frac{l_1}{l_2} \quad (23)$$

$$\gamma = \pi - \beta - \varphi \quad (24)$$

4.4. Summary of Requirements

The designing of the parameters of the safety architecture is done by numerical analysis and meets the required performance demands and found relationships:

- Required performance demands
  - Minimum required lifting stroke: 40 mm (ground clearance + wheel compression and lift)
  - Desired lifting force at contact patch: Fig. 4 (solid graph)
- Found relations by numerical analysis

- The longer the knee levers, the weaker the required actuation force
- Equal length of the levers leads to decreased spring stiffness: l_1=l_2
- The length of the levers is limited by the WMDS height and accessible linkage: l_1+l_2<540 mm

Furthermore the position of the safety architecture must prevent a rollover in case of maximum deceleration. Because the dimensioning of the motion base itself is designed to prevent a rollover, the positioning of the friction pads of the safety architecture underlies similar dimensioning constrains. Therefore the same base length of the equilateral triangle can be used. The necessary base length l_t of the WMDS Prototype becomes a function of the maximum friction coefficient μ_{max} and the height of the center of gravity (CG) h_{CG} (Fig.7). The most critical rollover condition occurs when the acceleration vector is perpendicular to any of the bases of the triangle. Hence the equation (25) is derived by setting up the balance of forces and calculating the moment equilibrium around point 2.

$$\sum_{(2)} M = 0 = m \cdot g \cdot (\mu_{max} \cdot h_{CG} - r_{ic}) + h_t \cdot F_{z,wheel,1} \quad (25)$$

$$r_{ic} = \frac{1}{3} h_t = \frac{1}{2\sqrt{3}} l_t \quad (26)$$

$$h_t = \frac{\sqrt{3}}{2} l_t \quad (27)$$

Rollover can be put on the same level as wheel lift, which occurs when the wheel load $F_{z,wheel,1}$ (28) becomes smaller than zero:

$$F_{z,wheel,1} = \frac{2 \cdot m \cdot g \cdot \left(\frac{1}{2\sqrt{3}} l_t - \mu_{max} \cdot h_{CG}\right)}{\sqrt{3} \cdot l_t} > 0 \quad (28)$$

$$\rightarrow l_t > 2\sqrt{3} \cdot \mu_{max} \cdot h_{CG} \quad (29)$$

Equation (29) defines the minimum base length needed to ensure rollover safety. With the dimensions of the WMDS Prototype shown in Table 1 the safety factor against rollover is 1.38.

Table 1: Geometric dimensions of the final WMDS Prototype

Parameter	Unit	Value
h_{CG}	mm	481
μ_{max}	mm	1
l_t	mm	2300
h_t	mm	1992

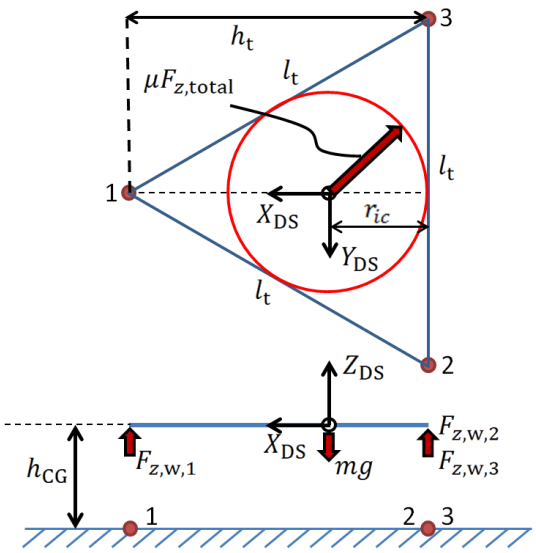

Fig. 7: Relation of sizing and rollover of the WMDS

4.5. Final Design

According to the derived constraints the dimensioning is calculated. The results are summarized in Table 2.

Table 2: Final design of the safety architecture

Parameter	Unit	Value
l_1	mm	270
l_2	mm	270
d_{joint}	mm	20
$\Delta s_{II,max}$	mm	102
α_{max}	°	3
α_{min}	°	0
φ_{max}	°	22
φ_{min}	°	0
c_{spring}	N/mm	67.58
$F_{des,max}$	N	8688[3]
$F_{spring,max}$	N	6970
μ_{slide}	./.	0.1[4]
μ_{joint}	./.	0.1[5]

The derived force transmission of the knee lever leads to the transformed desired lifting force (dashed graph) and actuation force of the linear spring used (dotted graph) as shown in Fig. 8. The created lifting system enables the application of a conventional spring while reducing the actuation force due to the transmission of force of the knee lever. Therefore, the effort for actively holding the preloaded spring is reduced significantly.

[3] Maximum wheel load with µ=1.45

[4] http://www.igus.de/wpck/2328/iglidur_Reibwerte, accessed: May 2014

[5] http://www.igus.de/wpck/2328/iglidur_Reibwerte, accessed: May 2014

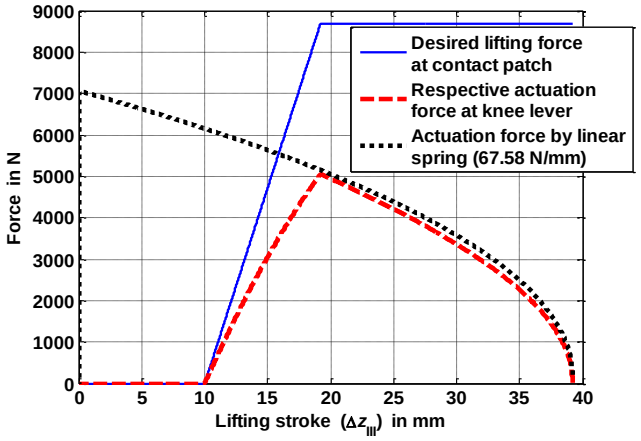

Fig. 8: Knee lever influence on force transmission ratio (knee levers: l_1=l_2=270 mm)

The specifications of the introduced safety architecture are summarized in Table 3.

Table 3: Specifications of the safety architecture

Parameter	Unit	Value
Lever arm of magnet	mm	470
Lever arm of spring	mm	250
Maximum magnetic force	N	4600
Actual magnetic force with applied anchor plate	N	4100
Supply voltage (of magnetic clamp)	V	24
Rated power (of magnetic clamp)	W	21
Maximum stroke of friction pad	mm	39
Shore hardness of friction pad	A °	70
Diameter of friction pad	mm	125

4.6. Parameter identification

In order to determine the sliding friction coefficient of the used braking pads, tests have been carried out. The WMDS with three discharged safety systems was pulled and the force needed for pulling was measured by a force sensor. The quotient of horizontal force and vertical force yields the sliding friction coefficient.

The tests were conducted with different velocities in order to identify the sensitivity of this parameter onto the friction coefficient. The mass of the prototype was increased to 1200 kg since this will be the maximum expected mass.

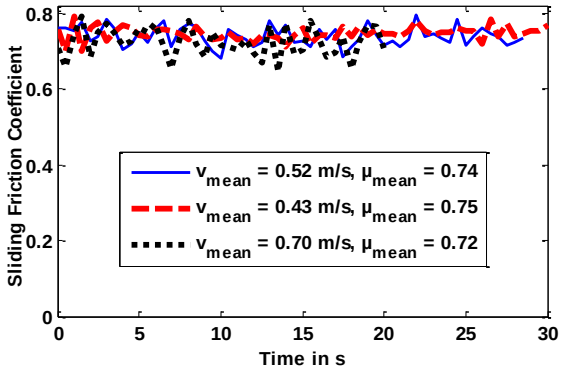

Fig. 9: Test results of sliding friction coefficient measurement with different velocities

As it can be seen in Fig. 9, the maximum average sliding friction coefficient within all measurements is about 0.75. The overall maximum value that has been recorded is 0.998. As sliding velocity increases, the sliding friction coefficient decreases. This behavior is known from rubber.

The wear of the friction pads is found to be tolerable. Over a sliding distance of approximately 100 m, the pad that is situated in the front (and therefore is prone to the highest wheel load) experiences a reduction in its height by 10 mm. Reducing the pad's height by 10 mm leads to ground contact of the wheels. This suggests that several emergency stops may occur before the friction pads have to be replaced.

4.7. Validation Tests

The concept of the safety architecture is validated by test drives utilizing the hardware prototype. The results are explained by one exemplary test drive. The measurement is conducted by a Correvit sensor and an acceleration based internal measurement unit (IMU).

The relevant part of the measurement is presented in Fig. 10. The deceleration due to the safety architecture starts at about 12.53 s. The acceleration signal shows a steep onset. At approx. 12.57 s the strong deceleration is paused for about 90 ms. The interruption is the result of a jump of the WMDS. For roughly 90 ms all contact patches are lifted from the ground due to the released energy of the safety architecture. The deceleration continues as soon as the friction pads are in ground contact again. The emergency stop lasts roughly 300 ms for the initial velocity of 2.4 m/s[6]. If the full emergency stop is considered, a mean deceleration of 7 m/s² is reached. If the jump

[6] Emergency stop at $v_{\text{initial}} = 2.4\,\text{m/s}$ to $v_{\text{correvit,min}} = 0.3\,\text{m/s}$ thus, 2.1 m/s are decelerated within 300 ms.

can be avoided, the mean deceleration is expected to be increased to about 7.5 m/s² according to the results of section 4.6. One possible approach to avoid the jump is to optimize the damping of the knee lever design. This measure is also expected to reduce the peak deceleration as the dynamic wheel load change of the friction elements is narrowed, causing less peak friction force. In Table 4 the results of the validation tests are summarized.

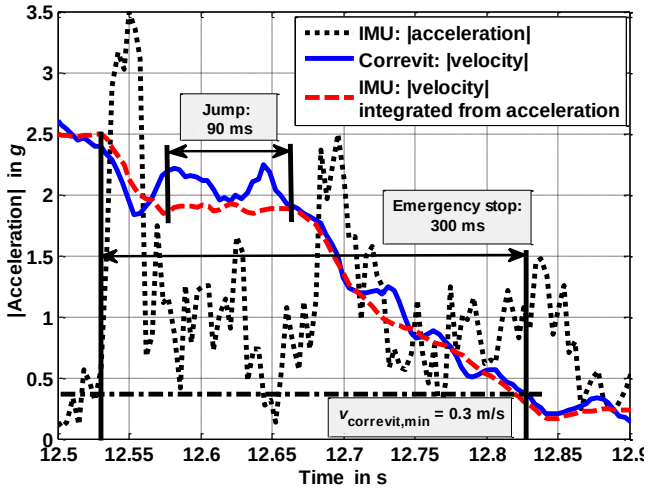

Fig. 10: Velocity and deceleration of WMDS during an emergency stop

Table 4: Characteristic values of the safety system's dynamics during an emergency stop

Property	Unit	Value
Initial velocity at discharge of the safety system	m/s	2.4
Duration of emergency stop (to $v_{\text{correvit,min}} = 0.3$ m/s)	ms	300
Duration of jump	ms	90
Mean deceleration	m/s²	7
Possible mean deceleration (no jump)	m/s²	7.5
Peak deceleration	m/s²	35

5. Conclusion

The safety architecture is validated by hardware testing. The clamping force enables the active hold of the preloaded spring. The knee lever reduces the required spring force and enables vertical stiffness when fully straightened (final position of knee lever in case of emergency stop). The utilized friction elements provide friction coefficient of about 0.75. The created mean deceleration of 7 m/s² is sufficient to stop the WMDS within an acceptable run-off area in case of an emergency. The wear of the elements must be observed further. The grit behavior seems to be promising because no spotty wear occurs. The grit has powdery characteristic and can be blown off. No significant marks remain. The first hardware tests show system jumps where the friction pads temporarily lose ground contact. Hence, future research will have to optimize the lifting process by suitable damping in order to reduce occurring wheel load change and thus create continuous friction force. The reduction of the peak deceleration yields reduced exposure of the subject and less mechanical stress for the safety system. Far-reaching improvements in terms of average power demand of the clamping task could be gained from alternative lifting concepts utilizing self-reinforcement. The basic idea of this improved safety architecture is being prepared for a patent application and will be analyzed in future research.

6. References

[Bet10] Betz, A.: Konzeption einer Bewegungsplattform eines selbstbewegten Fahrsimulators mit 6 DoF und dessen Umsetzung in ein evaluierbares Modell, Master's thesis, Insitute of Automotiv Engineering (Fachgebiet Fahrzeugtechnik), Technische Universität Darmstadt, Germany, 2010.

[Bet12a] Betz, A.; Winner, H.; Ancochea, M.; Graupner, M.: Motion Analysis of a Wheeled Mobile Driving Simulator for Urban Traffic Situations, Proceedings of Driving Simulation Conference 2012, p. 123-136, 6-7 September 2012 in Paris, France, 2012.

[Bet12b] Betz, A.; Hämisch, R.; Müller, M.; Winner, H.: Concept Analysis of a Wheeled Mobile Driving Simulator Showing an Omnidirectional Motion Base for Urban Traffic Simulation, SIMVEC - Berechnung, Simulation und Erprobung im Fahrzeugbau 2012, 20-21 November 2012 in Baden-Baden, Germany, 2012.

[Bet13] Betz, A.; Butry, A.; Junietz, P.; Wagner, P.; Winner, H.: Driving Dynamics Control of a Wheeled Mobile Driving Simulator Utilizing an Omnidirectional Motion Base for Urban Traffic Simulation. Future Active Safety Technology toward zero-traffic-accident (FASTzero). 22.-26. September 2013 in Nagoya, Japan. 2013.

[Bet14] Betz, A.: Feasibility Analysis and Design of Wheeled Mobile Driving Simulators for Urban Traffic Simulation, Dissertation (Ph.D.), 2014.

[Cla01] Clark, A.J.; Sparks, H.V.; Carmein, J.A.: Unique Features and Capabilities of the NADS Motion System, Proceedings of the 17th International Technical Conference on the En-

hanced Safety of Vehicles (ESV), 4-7 June 2001, Amsterdam, The Netherlands. 2001.

[Ker12] Kerle, H.; Corves, B.; Hüsing, M.: Getriebetechnik. Grundlagen, Entwicklung und Anwendung ungleichmäßig übersetzender Getriebe. 4th edition. Wiesbaden. 2012.

[Wag13] Wagner, P.: Aufbau und Inbetriebnahme eines selbstfahrenden Fahrsimulatorprüfstands, Master's thesis, Insitute of Automotiv Engineering (Fachgebiet Fahrzeugtechnik), Technische Universität Darmstadt, Germany, 2013.

[Wag14] Wagner, P.; Betz, A.; Winner, H.: Conception and design of mobile driving simulators, in Proceedings of the ASME 2014 International Design Engineering Technical Conferences & Computers and Information in Engineering Conference IDETC/CIE 2014, August 17-20, 2014 in Buffalo, NY, USA, 2014.

[Zee2010] Zeeb, E.: Daimler's New Full-Scale, High-dynamic Driving Simulator – A Technical Overview, Proceedings of the Driving Simulation Conference Europe 2010, p. 157-165, 9-10 September 2010 in Paris, France, 2010.

7. Appendix

Table 5: Summary of the safety system's properties

Parameter	Unit	Value
h_{CG}	mm	481
μ_{max}	mm	1
l_t	mm	2300
h_t	mm	1992
l_1	mm	270
l_2	mm	270
d_{joint}	mm	20
$\Delta s_{II,max}$	mm	102
α_{max}	°	3
α_{min}	°	0
φ_{max}	°	22
φ_{min}	°	0
c_{spring}	N/mm	67.58
$F_{des,max}$	N	8688[7]
$F_{spring,max}$	N	6970
μ_{slide}	./.	0.1[8]
μ_{joint}	./.	0.1[9]
Lever arm of magnet	mm	470
Lever arm of spring	mm	250
Maximum magnetic force	N	4600
Actual magnetic force with applied anchor plate	N	4100
Supply voltage (of magnetic clamp)	V	24
Rated power (of magnetic clamp)	W	21
Maximum stroke of friction pad	mm	39
Shore hardness of friction pad	A °	70
Diameter of friction pad	mm	125
Initial velocity at discharge of the safety system	m/s	2.4
Duration of emergency stop (to $v_{correvit,min} = 0.3$ m/s)	ms	300
Duration of jump	ms	90
Mean deceleration	m/s²	7
Possible mean deceleration (no jump)	m/s²	up to 10
Peak deceleration	m/s²	35

[7] Maximum wheel load with μ=1.45

[8] http://www.igus.de/wpck/2328/iglidur_Reibwerte, accessed: May 2014

[9] http://www.igus.de/wpck/2328/iglidur_Reibwerte, accessed: May 2014